

JGR Atmospheres

RESEARCH ARTICLE

10.1029/2018JD029998

Key Points:

- The magnitude of the M-component electric field at 15 km is not sensitive to the speed of the M-component current wave, while it increases significantly with increasing the branch-to-channel junction point height
- At 15 km, the electric field associated with M-component-type pulses is dominated by the electrostatic component and the magnetic field by the induction component
- The effect of mountainous terrain on propagation of electromagnetic field of M-component-type pulses depends on the branch-to-channel junction point height

Correspondence to:

F. Rachidi,
farhad.rachidi@epfl.ch

Citation:

He, L., Rachidi, F., Azadifar, M., Rubinstein, M., Rakov, V. A., Cooray, V., et al (2019). Electromagnetic fields associated with the M-component mode of charge transfer. *Journal of Geophysical Research: Atmospheres*, 124, 6791–6809. <https://doi.org/10.1029/2018JD029998>







Received 14 NOV 2018

Accepted 26 APR 2019

Accepted article online 17 MAY 2019

Published online 4 JUL 2019

Electromagnetic Fields Associated With the M-Component Mode of Charge Transfer

Lixia He^{1,2} , Farhad Rachidi² , Mohammad Azadifar^{2,3} , Marcos Rubinstein³ , Vladimir A. Rakov^{4,5} , Vernon Cooray⁶, Davide Pavanello⁷ , and Hongyan Xing¹

¹Collaborative Innovation Center on Forecast and Evaluation of Meteorological Disasters (CIC-FEMD), Jiangsu Key Laboratory of Meteorological Observation and Information Processing, Nanjing University of Information Science and Technology, Nanjing, China, ²Electromagnetic Compatibility Laboratory, Swiss Federal Institute of Technology (EPFL), Lausanne, Switzerland, ³Institute of Information and Communication Technologies, University of Applied Sciences of Western Switzerland, Yverdon-les-Bains, Switzerland, ⁴Department of Electrical and Computer Engineering, University of Florida, Gainesville, FL, USA, ⁵Moscow Institute of Electronics and Mathematics, National Research University Higher School of Economics, Moscow, Russia, ⁶Division for Electricity, Uppsala University, Uppsala, Sweden, ⁷Institute of Sustainable Energy, University of Applied Sciences of Western Switzerland (HES-SO), Sion, Switzerland

Abstract In upward flashes, charge transfer to ground largely takes place during the initial continuous current (ICC) and its superimposed pulses (ICC pulses). ICC pulses can be associated with either M-component or leader/return-stroke-like modes of charge transfer to ground. In the latter case, the downward leader/return stroke process is believed to take place in a decayed branch or a newly created channel connected to the ICC-carrying channel at relatively short distance from the tower top, resulting in the so-called mixed mode of charge transfer to ground. In this paper, we study the electromagnetic fields associated with the M-component charge transfer mode using simultaneous records of electric fields and currents associated with upward flashes initiated from the Säntis Tower. The effect of the mountainous terrain on the propagation of electromagnetic fields associated with the M-component charge transfer mode (including classical M-component pulses and M-component-type pulses superimposed on the initial continuous current) is analyzed and compared with its effect on the fields associated with the return stroke (occurring after the extinction of the ICC) and mixed charge transfer modes. For the analysis, we use a 2-Dimensional Finite-Difference Time Domain method, in which the M-component is modeled by the superposition of a downward current wave and an upward current wave resulting from the reflection at the bottom of the lightning channel (Rakov et al., 1995, <https://doi.org/10.1029/95JD01924> model) and the return stroke and mixed mode are modeled adopting the MTLE (Modified Transmission Line with Exponential Current Decay with Height) model. The finite ground conductivity and the mountainous propagation terrain between the Säntis Tower and the field sensor located 15 km away at Herisau are taken into account. The effects of the mountainous path on the electromagnetic fields are examined for *classical* M-component and M-component-type ICC pulses. Use is made of the propagation factors defined as the ratio of the electric or magnetic field peak evaluated along the mountainous terrain to the field peak evaluated for a flat terrain. The velocity of the M-component pulse is found to have a significant effect on the risetime of the electromagnetic fields. A faster traveling wave speed results in larger peaks for the magnetic field. However, the peak of the electric field appears to be insensitive to the M-component wave speed. This can be explained by the fact that at 15 km, the electric field is still dominated by the static component, which mainly depends on the overall transferred charge. The contribution of the radiation component to the M-component fields at 100 km accounts for about 77% of the peak electric field and 81% of the peak magnetic field, considerably lower compared to the contribution of the radiation component to the return stroke fields at the same distance. The simulation results show that neither the electric nor the magnetic field propagation factors are very sensitive to the risetimes of the current pulses. However, the results indicate a high variability of the propagation factors as a function of the branch-to-channel junction point height. For junction point heights of about 1 km, the propagation factors reach a value of about 1.6 for the E-field and 1.9 for the H-field. For a junction height greater than 6 km, the E-field factor becomes slightly lower than 1. The obtained results are consistent with the findings of Li, Azadifar, Rachidi, Rubinstein, Paolone, et al. (2016, <https://doi.org/10.1109/TEMC.2015.2483018>) in which an electric field propagation factor of 1.8 was inferred for return strokes and mixed-mode pulses, considering that junction points lower than 1 km or so would result in a mixed mode of charge transfer, in which a downward leader/return-stroke-like process is

believed to take place. It is also found that the field enhancement (propagation factor) for return stroke mode is higher for larger ground conductivities. Furthermore, the enhancement effect tends to decrease with increasing current risetime, except for very short risetimes (less than 2.5 μ s or so) for which the tendency reverses. Finally, model-predicted fields associated with different charge transfer modes, namely, return stroke, mixed-mode, classical M-component, and M-component-type ICC pulse are compared with experimental observations at the Säntis Tower. It is found that the vertical electric field waveforms computed considering the mountainous terrain are in very good agreement with the observed data. The adopted parameters of the models that provide the best match with the measured field waveforms were consistent with observations. The values for the current decay height constant adopted in the return stroke and mixed-mode models (1.0 km for the return stroke and 0.8 km for the mixed-mode pulse) are lower than the value of 2.0 km typically used in the literature.

1. Introduction

M components are perturbations (or surges) in the relatively steady continuing current and in the associated channel luminosity. The M in the term M component stands for D. J. Malan (Malan & Collens, 1937) who was the first to study this lightning process. *Classical* M components occur in downward lightning and involve a single channel between the cloud base and ground. They are excited at the upper extremity of the channel (in the cloud) by either recoil leaders or separate in-cloud leaders coming in contact with the grounded current-carrying channel. Recoil leaders are thought to occur in decayed channel branches previously supplying current to the grounded channel. Similar to leader/return stroke sequences and to continuing currents in negative lightning, M components serve to transport negative electric charge from the cloud to ground. The M-component mode of charge transfer to ground differs from the dart leader/return stroke mode in that the former requires the presence of a current-carrying channel to ground, while the latter apparently occurs along the remnants of the previously formed channel when there is essentially no current (above 0.1–2 A) flowing to ground. M-component-like processes also occur during the initial stage of object-initiated and rocket-triggered lightning, when a steady-current-carrying channel is excited at a height of a kilometer or more above its ground termination point. Further information about M-component mode of charge transfer to ground is found in section 4.8 of Rakov (2016c).

Direct measurements of lightning currents can be obtained either using instrumented towers (e.g., Berger, 1975; Diendorfer et al., 2009; Heidler et al., 2015; Romero et al., 2013; Visacro et al., 2004) or using artificial initiation of lightning from natural thunderclouds (e.g., Qie et al., 2011; Thottappillil et al., 1995). Besides, information on lightning current can be remotely inferred from lightning location systems using empirical (e.g., Rakov et al., 1992) or theoretical (e.g., He et al., 2014; Rachidi & Thottappillil, 1993; Zhang et al., 2014) equations. The estimation of lightning current parameters from remote field measurements is affected by the conditions of the propagation path of the electromagnetic fields. Lightning electromagnetic fields experience attenuation and distortion when propagating along a lossy ground (e.g., Cooray et al., 2012). Many researchers have proposed approximate expressions to estimate the attenuation and distortion of electromagnetic fields due to the finitely conducting ground, considering either a homogeneous or a stratified soil (see Shoory et al., 2012, for a review).

The Finite-Difference Time Domain (FDTD) approach (Yee, 1966) has been widely used for calculating lightning electromagnetic fields generated at different distances from as close as tens/hundreds of meters (Baba & Rakov, 2007a; Mimouni et al., 2008) to as far as hundreds to thousands of kilometers (Berenger, 2005; Tran et al., 2017). The FDTD approach is often employed as a reference method to validate approximate expressions proposed for the computation of lightning electromagnetic fields (e.g., Khosravi-Farsani et al., 2013; Shoory et al., 2011). It has also been used to evaluate the influence of the struck object (e.g., Baba & Rakov, 2008), the building on which field sensors are located (e.g., Baba & Rakov, 2007b), and irregular terrain (e.g., Kobayashi et al., 2016; Li et al., 2014; Li, Azadifar, Rachidi, Rubinstein, Diendorfer, et al., 2016; Li, Azadifar, Rachidi, Rubinstein, Paolone, et al., 2016; Oikawa et al., 2013; Soto et al., 2014).

In lightning strikes to ground or to a tall structure, the mode of charge transfer to ground has a significant influence on the lightning current and electromagnetic fields. In downward flashes, electric charges can be transferred to ground via three different modes: downward leader/return-stroke sequence, continuing current, and M component (Rakov et al., 2001). In upward flashes, charge transfer to ground essentially

takes place during the initial continuous current (ICC) and its superimposed pulses (ICC pulses). ICC pulses can be associated with either M-component or leader/return-stroke-like modes of charge transfer to ground (Zhou et al., 2015). In this latter case, called mixed mode of charge transfer to ground (Zhou et al., 2011), the downward leader/return stroke process is believed to take place in a decayed branch or a newly created channel connected to the ICC-carrying channel at relatively short distance from the tower top. M-component-type ICC pulses are presumably associated with the reactivation of a decayed branch or the connection of a newly created channel to the ICC-carrying channel at larger junction heights. After the extinction of the ICC, charge transfer to ground can take place via either return strokes, which are preceded by an essentially no-current interval, or classical M-component mode pulses that are superimposed on the continuing current after some return-stroke pulses. Typical waveforms of each type will be shown in section 5 of the paper.

The analysis presented by He, Azadifar, Rachidi, et al. (2018) suggests that the M-component-type pulses during the initial stage (ICC) have very similar characteristics to those of classical M-component pulses occurring during the continuing current (CC) after some return strokes. Their study also confirmed the similarity of mixed-mode pulses and return strokes, as already suggested in other studies (e.g., Azadifar et al., 2016; Flache et al., 2009; Zhou et al., 2015).

He, Azadifar, Rachidi, et al. (2018) also proposed a new criterion based on the current waveform symmetry to distinguish between mixed-mode pulses and M-component-type pulses, the latter exhibiting a more symmetrical waveform than the former.

In this paper, we analyze the propagation effects on the electric fields associated with different charge transfer modes using simultaneous records of electric fields and currents associated with upward flashes to the Sântis Tower. For the analysis, we use a 2-D FDTD (2-Dimensional Finite-Difference Time Domain) method, in which the return stroke and mixed mode are modeled adopting the modified transmission line model with current decaying exponentially with height (MTLE; Nucci et al., 1988; Rachidi & Nucci, 1990), and the M component is modeled by the superposition of a downward current wave and an upward wave resulting from the reflection at the bottom of the lightning channel (Rakov et al., 1995; Rakov et al., 2001). The finite ground conductivity and the mountainous terrain between the Sântis Tower and the field sensor located 15 km away at Herisau are taken into account. The effects of the mountainous propagation path on the electromagnetic fields are examined for the four types of lightning pulses.

The rest of the paper is organized as follows. Section 2 describes the current measurement system at the Sântis Tower and the electric field measuring system in Herisau, approximately 15 km away from the tower. Section 3 describes the adopted models and the simulation approach. Section 4 presents the simulation results and discussion, with emphasis on the propagation effects along mountainous terrain on the electromagnetic field generated by M-component-type pulses. For comparison, the propagation effect on the fields associated with the return-stroke charge transfer mode is studied as well. Section 5 presents a comparison between model-predicted fields and observations. Finally, a summary and conclusions are given in section 6.

Throughout the paper, a positive sign for the current is used for negative return strokes, and the atmospheric electricity sign convention (downward directed electric fields or electric field change vectors are positive) is adopted for the electric field.

2. Instrumentation and Data Set

2.1. Lightning Current and Electric Field Measuring Systems

The Sântis Tower was instrumented in May 2010 for lightning current measurements. The tower is equipped with two sets of instruments, each including a Rogowski coil and a multigap B-Dot sensor, mounted at two heights along the tower, 24 and 82 m above ground level (Azadifar et al., 2014; Romero et al., 2010).

The electric field-measuring system is located about 15 km away from the Sântis Tower, installed on the roof of a 25-m tall building in Herisau. It comprises a flat-plate antenna and an analog integrator with an overall frequency bandwidth of 40 Hz to 2 MHz. The decay time constant of the integrator is about 4.2 ms, so its effect on the fields in the considered time windows (maximum 1.5 ms) is expected to be insignificant. The signal is digitized and recorded using a PCI 5122 National Instruments card with sampling rate of 5 MS/s and a time window of 4 s.

It is known that the building on top of which the measuring sensors are located can affect the measured signals (Baba & Rakov, 2007b; Mosaddeghi et al., 2009). For example, Baba and Rakov (2007b) have shown that a 20-m tall building can result in an enhancement factor of 1.5. However, the effect depends strongly on the local configuration. The building in Herisau, on which the field sensor was located, is surrounded by similar buildings, making in situ calibration difficult. Simulation results and comparison with experimental data suggest that the enhancement factor should be close to 1 (Li, Azadifar, Rachidi, Rubinstein, Diendorfer, et al., 2016).

2.2. Data Set

The data set is composed of simultaneous records of currents and vertical electric field waveforms associated with two upward negative flashes initiated from the Sântis Tower on 18 August 2016 at 15:38:58 and at 18:49:29 local time, respectively. One event for each category of pulses, namely, return-stroke pulse, mixed-mode pulse, M-component-type ICC pulse, and M-component pulse, was considered as reference for the analysis to validate the simulation models.

Because the GPS system was not working properly during these two flashes, the current pulses and the associated electric field pulses of each flash were synchronized manually by aligning the current peak and the associated field peak of the last return stroke. The alignment error was evaluated to be on the order of a few microseconds (Li, Azadifar, Rachidi, Rubinstein, Paolone, et al., 2016).

3. Modeling

3.1. Model for the Classical M Components and M-Component-Type ICC Pulses

The model of Rakov et al. (1995, 2001) was used for the modeling of M components and M-component-type ICC pulses. In this model, which assumes a purely vertical and straight channel, the initial current distribution is defined as an incident current wave launched at the junction point between an in-cloud leader channel and the current-carrying channel to ground, moving downward. When the current wave reaches the base of the channel, a reflected wave is produced, which travels upward. As a result, the overall current distribution becomes a superposition of two waves moving in opposite directions. Both the incident downward wave and the reflected upward wave are assumed to travel at a constant speed and undistorted. The distribution of the M-component mode current along the ICC- or the continuing-current-carrying channel is expressed as

$$\begin{aligned} i(z', t) &= i(h_m, t - (h_m - z')/v_m) & t < h_m/v_m \\ i(z', t) &= i(h_m, t - (h_m - z')/v_m) + i(h_m, t - (h_m + z')/v_m)\rho_g & t \geq h_m/v_m \end{aligned} \quad (1)$$

where v_m is the velocity of the M-component current wave, h_m is the current height of the junction point between the leader and the ICC/CC-carrying channel above the Sântis Tower top, and ρ_g is the reflection coefficient at the ground. It is worth noting that in (1), the presence of the tower was neglected, assuming that its height is electrically small and, therefore, the effective reflection experienced by the downward wave is determined by the ground reflection coefficient. Current distributions given by (1) apply to both the 124-m tower and lightning channel attached to its top. The two-wave M-component model is supported by field observations at close distances (30–500 m) in Florida (Rakov et al., 1995, 2001) and at longer distances (e.g., 15 km in He, Azadifar, Li, et al., 2018).

3.2. Model for Return-Stroke and Mixed-Mode Pulses

The adopted model for the return-stroke pulses is the modified transmission line model with current decaying exponentially with height (MTLE; Nucci et al., 1988; Rachidi & Nucci, 1990). We will use the same model for mixed-mode pulses because of their similar characteristics to those of return strokes (Azadifar et al., 2016) and also because the junction point height for mixed-mode pulses is lower than 1 km according to the study of Zhou et al. (2015). In this case, the contribution of the downward leader-like current wave to the fields at 15-km distance is negligible. According to the MTLE model, the current distribution along the channel is defined as

$$\begin{aligned} i(z', t) &= i(0, t - z'/v_{rs}) \exp(-z'/\lambda) & t \geq z'/v_{rs} \\ i(z', t) &= 0 & t < z'/v_{rs} \end{aligned} \quad (2)$$

where v_{rs} is the return stroke speed and λ is the current attenuation height constant. In (2), reflection from the tower top and the transient process occurring along the tower were not considered (assuming that the

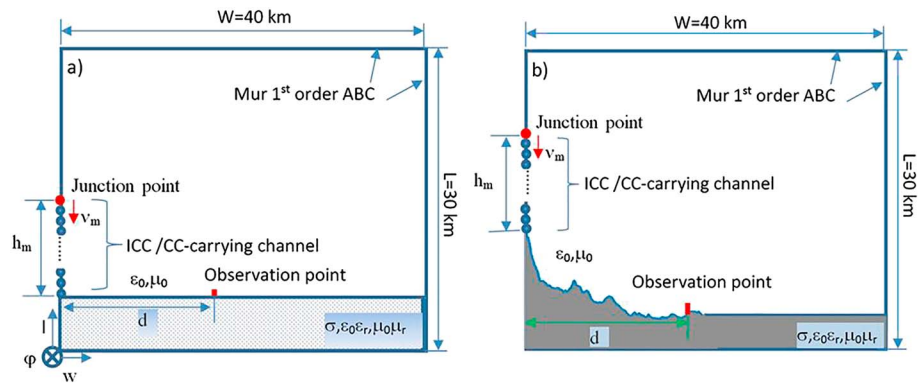


Figure 1. Geometry of the 2-D cylindrical FDTD simulation domain for the evaluation of the electromagnetic fields generated by M-component-type pulses (classical M-component pulses and M-component-type ICC pulses). (a) Assuming a flat ground and (b) considering the 2-D terrain topography between the Säntis Tower and the field observation site in Herisau.

tower is electrically short and its impedance is the same as the characteristic impedance of the lightning channel). In the case of a tall tower, engineering models including MTLE have been extended to account for such transients (e.g., Baba & Rakov, 2005; Rachidi et al., 2002).

3.3. Electromagnetic Field Computation

In this study, we employ a 2-D cylindrical FDTD approach (Yee, 1966) to simulate the electromagnetic fields generated by either (i) M-component-type pulses (including classical M-component pulses and M-component-type ICC pulses) or (ii) return-stroke pulses and mixed-mode pulses. The two simulation models are shown in Figures 1 and 2, respectively. The current distribution along the channel for each model (equations (1) and (2)) is specified in the FDTD model using a phased current source array (Baba & Rakov, 2003). The electromagnetic fields are computed considering two different propagation paths, namely, (1) assuming the propagation path between the Säntis Tower and the field measurement point in Herisau to be a flat, homogeneous lossy ground (Figures 1a and 2a) and (2) taking into account the actual topography of the terrain (Figures 1b and 2b). The adopted approach is similar to the one used by Li, Azadifar, Rachidi, Rubinstein, Paolone, et al. (2016) in which in order to reduce the computational burden associated with a 3-D FDTD approach, a 2-D axial symmetric configuration, based on the two-dimensional topographic map along the direct path between the Säntis Tower and the field measurement station, was used. We have adopted a 2-D axial symmetric FDTD model that assumes that the 2-D cross section of the topographic map along the direct path between the Säntis Tower and the Herisau station is the same in all azimuthal directions. This assumption is discussed in detail in Li et al. (2017) where it is shown that the 2-D axial-symmetric

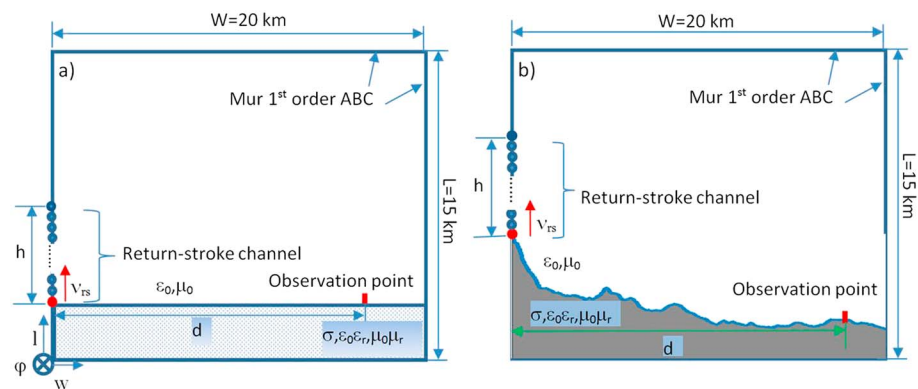


Figure 2. Geometry of the 2-D cylindrical FDTD simulation domain for the evaluation of the electromagnetic fields generated by return-stroke-type pulses (return-stroke pulses and mixed-mode pulses). (a) Assuming a flat ground and (b) considering the 2-D terrain topography between the Säntis Tower and the field observation site in Herisau.

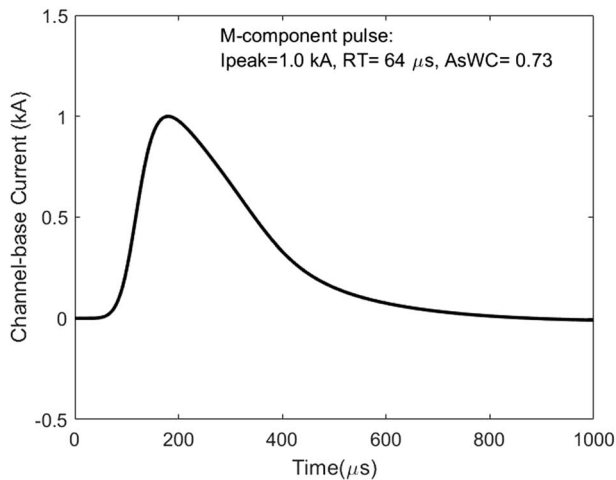


Figure 3. M-component channel base current waveform.

FDTD model can provide a good accuracy with respect to results obtained using a 3-D FDTD approach while considerably reducing computation time. Of course, the 2-D axial-symmetric analysis might lead to inaccuracies in the cases when the terrain is characterized by a particularly strong radial asymmetry.

It should also be mentioned that we have not considered the effect of the soil stratification along the considered field propagation path, which depends on the depth of the top layer and electrical characteristics of the layers (Li et al., 2019; Zhang et al., 2012).

Figure 1 shows the geometry of two-dimensional cylindrical coordinate FDTD simulation domains for the computation of the electromagnetic field generated by M-component-type pulses. The red-filled circles indicate the initial injection point of the M-component-type pulses, and the red arrows indicate the propagation direction of the initial current wave. In accordance with equation (1), v_m is the velocity of the M component, h_m is the branch-to-channel junction point height (hereafter referred as junction point height) of the in-cloud leader channel, and d is the distance

between the lightning channel and the field sensor at Herisau (the red-filled rectangle). W and L are the radial and vertical sizes of the two-dimensional computational domain, respectively. The domain shown in Figure 1a represents the ground as a flat conducting half-space with constant electrical parameters, while the domain shown in Figure 1b takes into account the mountainous terrain between the Säntis Tower and the observation point considering the 2-D terrain topography obtained from ASTER GDEM version 002 (Meyer, 2011), as in Li, Azadifar, Rachidi, Rubinstein, Paolone, et al. (2016). A first-order Mur Absorbing Boundary Condition (Mur, 1981) was employed to truncate the computational domain without causing reflections. ϵ_0 and μ_0 are the permittivity and permeability of free space, and σ , ϵ_r , and μ_r are the conductivity, relative permittivity, and relative permeability of the ground.

The adopted simulation domain for the two-dimensional FDTD is 40 km (along the radial axis, W in Figure 1) \times 30 km (along the vertical axis, L in Figure 1). The space is divided into square cells of 20 m \times 20 m with a time step $\Delta t = 33.3$ ns.

Figure 2 shows the geometry of two-dimensional cylindrical coordinate FDTD simulation domains for the computation of the electromagnetic field generated by return-stroke-type pulses. Red filled circles indicate the initial injection points of return-stroke-type pulses, and red arrows indicate the propagation direction of the initial current. As shown in equation (2), v_{rs} is the velocity of the return-stroke-type pulses, and h is the height of the channel. Considering the fact that return strokes and mixed-mode pulses are characterized by much faster rising waveforms compared to M components and M-component-type ICC pulses, the adopted simulation domain is 20 km (radial W axis) \times 15 km (vertical L axis), which is divided into square cells of 5 m \times 5 m with a time step $\Delta t = 8.33$ ns. Other parameters are the same as in Figure 1.

Three finite ground conductivities, $\sigma = 10, 1,$ and 0.1 mS/m, were considered in the simulations. ϵ_r and μ_r were assumed to be equal to 10 and 1, respectively.

The simulation models were validated using as reference closed-form time domain solutions (Uman et al., 1975) for the case of a flat, perfectly conducting ground and also numerical simulations published by Li, Azadifar, Rachidi, Rubinstein, Paolone, et al. (2016) for the case of a mountainous terrain. The validation results are not shown here for the sake of brevity.

4. Characteristics of Electromagnetic Field Pulses Associated With M-Component Pulses and M-Component-Type ICC Pulses

4.1. Current Distribution Along the Channel

We have considered a typical M-component channel base current waveform shown in Figure 3. The current associated with the M-component mode of charge transfer to ground has a more or less symmetrical waveform (Rakov et al., 2001). He, Azadifar, Rachidi, et al. (2018) proposed to use a coefficient called asymmetrical waveform coefficient (AsWC) to distinguish between M-component-type ICC pulses and mixed-mode

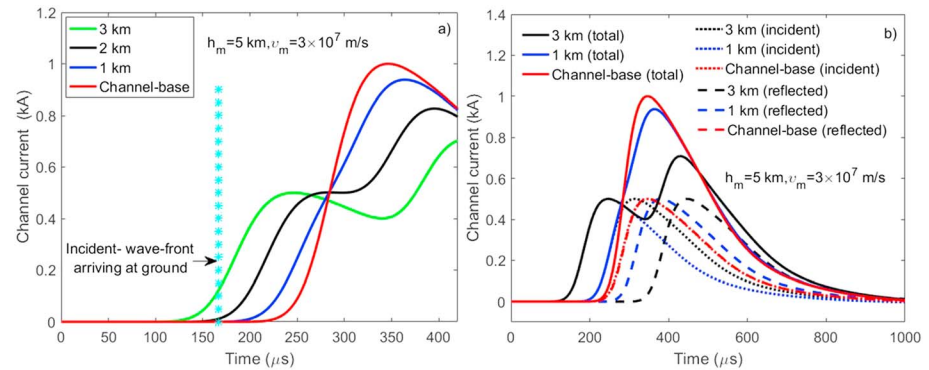


Figure 4. Current distribution in the ICC/CC-carrying channel associated with an M-component charge transfer mode (the channel base current is shown in Figure 3). The junction point is at a height of 5 km, the velocity of the traveling M-component wave is assumed to be 3×10^7 m/s, and the ground reflection coefficient for current is assumed to be 1.0. (a) Current waveforms at different heights along the channel. (b) Decomposition of current waveforms into incident (dotted curves) and ground-reflected (dashed curves) currents.

pulses by quantifying the asymmetry of the observed current pulses. The AsWC is defined as (He, Azadifar, Rachidi, et al., 2018)

$$AsWC = \frac{FWHM - t_{50\% - 100\%}}{FWHM} \quad (3)$$

where $t_{50\% - 100\%}$ is the time interval during which the current rises from 50 to 100% of its peak value and FWHM is the full width at half maximum.

A fully symmetrical pulse is characterized by an AsWC equal to 1/2, while waveforms characteristic of return strokes or mixed modes have AsWCs close to 1.0. According to He, Azadifar, Rachidi, et al. (2018), if AsWC for a pulse superimposed on the ICC is lower than 0.8, the pulse is classified as an M-component-type ICC pulse. As an example, the pulse presented in Figure 3 is characterized by a risetime of 64 ms and an AsWC of 0.73, typical of M-component and M-component-type ICC pulses observed at the Sântis Tower, according to the measurements presented in He, Azadifar, Rachidi, et al. (2018).

Figure 4 shows the distribution of the M-component current along the ICC/CC-carrying channel as predicted by the model of Rakov et al. (1995, 2001) equations (1). The junction point is assumed to be at a height of 5 km (Rakov et al., 1995), the traveling speed of the M-component current is assumed to be 3×10^7 m/s (Rakov et al., 1995), and the ground reflection coefficient for current is assumed to be 1.0. From Figures 4a and 4b, one can see that the channel base current is characterized by the highest peak, twice the incident current as a result of a full reflection at ground (ground reflection coefficient $\rho_g = 1.0$). The currents along the channel are characterized by an initial peak, which is due to the incident wave, and after a time corresponding to the wave traveltime from the observation point to ground and back, the ground-reflected wave adds up to it. The higher the observation point along the channel, the later the contribution of the ground-reflected wave and the smaller the overall current peak value (until the peaks of incident and reflected waves become fully separated in time).

4.2. Electromagnetic Fields Over a Flat, Perfectly Conducting Ground

Characteristics of the electromagnetic fields generated by an M component at close distances (30 to 500 m) have been discussed in Rakov et al. (1995, 2001). Here we briefly discuss the characteristics of electromagnetic fields generated by M-component-type pulses at relatively far distances: (i) 15 km, the distance at which the electric field was recorded, and (ii) 100 km, a typical distance at which electromagnetic fields were characterized in different studies. The electric field signatures of M components within a few kilometers of the lightning channel are V-shaped (for the case of negative charge transfer to ground, a negative excursion is followed by a positive excursion; atmospheric electricity sign convention; e.g., Rakov, 2016b, p. 236). In contrast, at larger distances, the signatures appear as ramps.

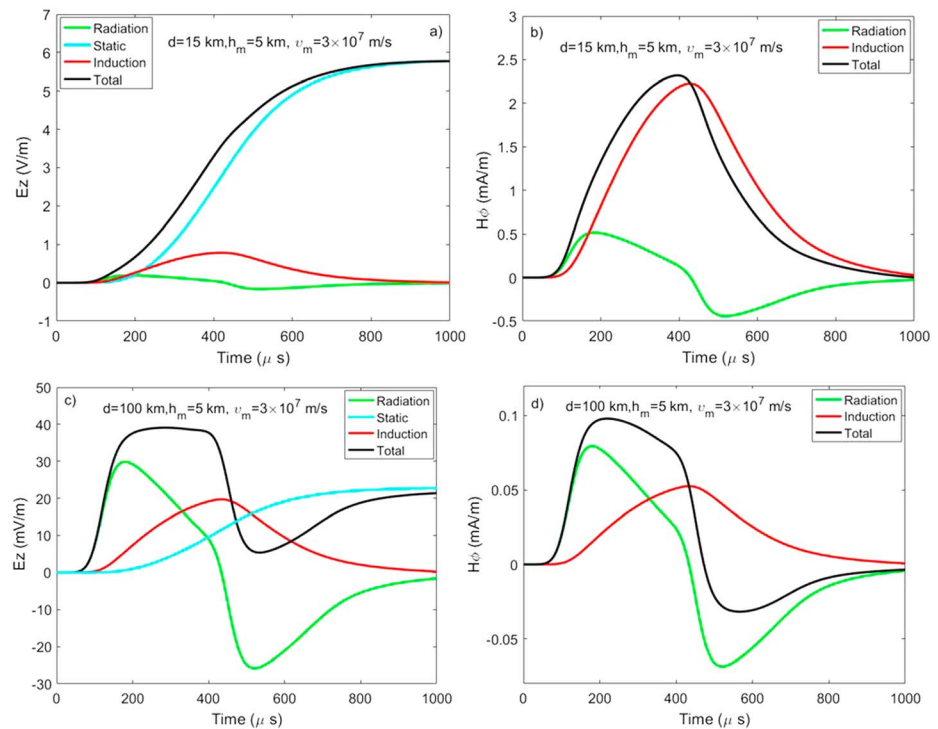


Figure 5. Vertical electric field (a and c) and azimuthal magnetic field (b and d) associated with the M-component charge transfer mode (the channel base current is shown in Figure 3). Top panels (a and b): fields calculated at 15 km. Bottom panels (c and d): fields calculated at 100 km. In each figure, the contribution of the field components (static, induction, and radiation for the E-field and induction and radiation for the H-field) is also shown. The same junction-point height and M-current wave front speed as in Figure 4 are adopted.

Figure 5 presents the vertical electric field and azimuthal magnetic field calculated at distances of 15 and 100 km from the ICC/CC-carrying channel. We have also shown for each case the contribution of the field components, namely, the static, induction, and radiation components for the electric field and the induction and radiation components for the magnetic field. It should be noted that the electromagnetic fields at 15 and 100 km presented in Figure 5 are calculated by using the analytical expressions (equations 7 and 9 in Uman et al., 1975), not the FDTD approach. The calculations have been performed assuming the channel base current shown in Figure 3 and adopting the same values as in Figure 4 for the height of the junction point, the velocity of the M-component current, and the ground reflection coefficient. From Figures 5a and 5b, one can see that the radiation component of the field does not play a significant role in the fields at 15 km. The vertical

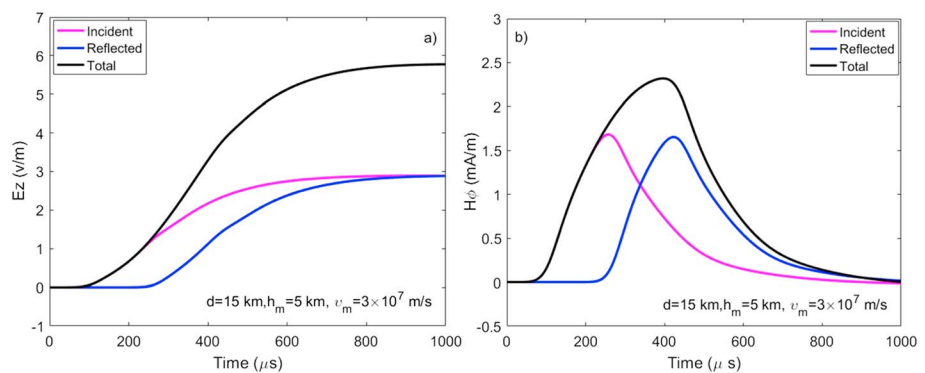


Figure 6. Vertical electric field (a) and azimuthal magnetic field (b) at 15 km from the ICC/CC-carrying channel associated with the M-component charge transfer mode pulse (the channel base current is shown in Figure 3). The contribution of the incident wave is given in the pink curves and that of the ground-reflected wave in blue. The black curves represent total fields. The same junction-point height and M-current wave front speed as in Figure 4 are adopted.

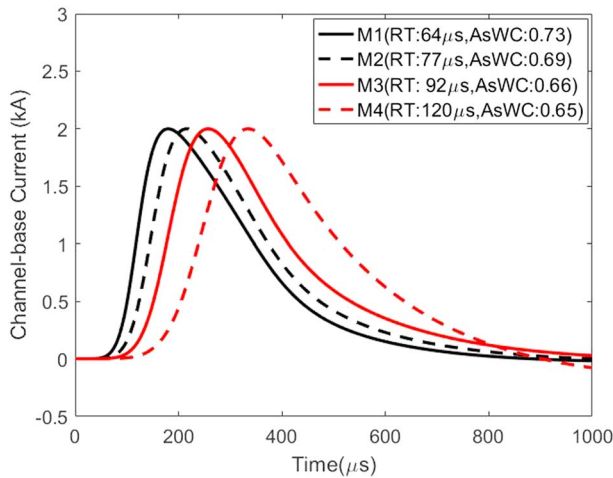


Figure 7. Adopted current waveforms for M-component and M-component-type ICC pulses. The parameters of the four waveforms were chosen based on the study of He, Azadifar, Rachidi, et al. (2018).

electric field is essentially dominated by the static component and the magnetic field by the induction component. This is in contrast with fields generated by return strokes, which are dominated at early times by their radiation terms at similar distances (e.g., Rachidi & Thottappillil, 1993). On the other hand, the contribution of the radiation component to the fields at 100-km distance becomes significant, accounting for about 77% of the peak electric field and 81% of the peak magnetic field. The fact that the radiation field is not dominant at distances as large as 15 km is essentially due to the relatively long risetime and slow speed of the M-component current wave. The fact that the fields are dominated by the static and induction components results in a faster decay of the M-component fields with increasing of the distance, compared to the $1/r$ decay of radiation fields. It is interesting to note that the magnetic field waveform at 100 km is bipolar, while the electric field waveform is not. This is because of the contribution of the static component to the E-field, which is still important at this distance. It should be noted, however, that for faster-rising currents, such as the one presented in Figure 5 of Pichler et al. (2010), the E-field can feature a bipolar waveform as well.

Figure 6 presents the contributions of the incident downward wave and the ground-reflected wave to the overall electric and magnetic fields computed at 15 km. As can be seen from the figure, the reflected current wave at ground produces a positive contribution to the field, which comes after a time delay corresponding to the propagation of the downward wave from the junction point to ground, as seen at the observation point.

4.3. Propagation Effects Along Mountainous Terrain

The effect of the mountainous terrain on the propagation of electromagnetic fields from lightning return strokes to the Säntis Tower was analyzed by Li, Azadifar, Rachidi, Rubinstein, Paolone, et al. (2016). The main conclusion of the study of Li et al. was that the propagation of the electric field generated by return-stroke-type pulses along the mountainous terrain between the Säntis Tower and the field observation point resulted in a significant enhancement of the fields, compared to the case of the propagation along a flat ground.

In this section, we will analyze the effect of the propagation along the mountainous terrain between the Säntis Tower and the field observation point at Herisau for classical M-component and M-component-type ICC pulses. As we have seen in the previous section, the fields for M-component mode of charge transfer

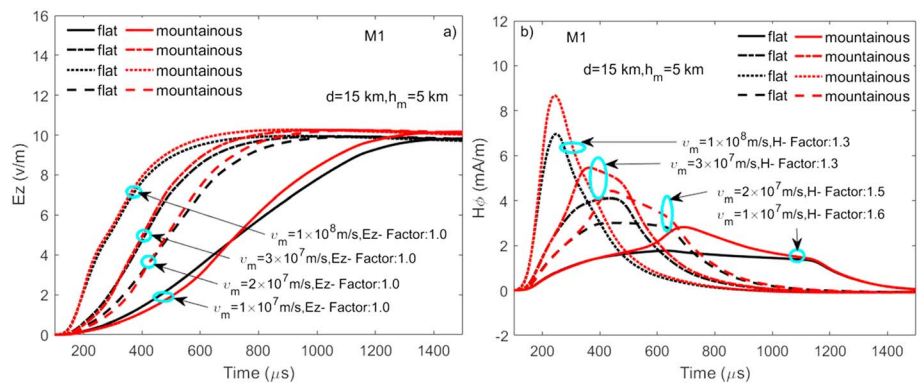


Figure 8. Vertical electric field (a) and azimuthal magnetic field (b) at 15 km associated with the M-component-type pulse M1 (shown in Figure 7), calculated for different velocities (1×10^7 , 2×10^7 , 3×10^7 , and 1×10^8 m/s). Black curves: simulated fields assuming a flat lossy ground. Red curves: simulated fields considering the mountainous topography between the Säntis Tower and the field measurement sensor in Herisau. Junction point height $h_m = 5$ km. Ground reflection coefficient $\rho_g = 0.8$. Ground electrical parameters: $\sigma = 1$ mS/m, $\epsilon_r = 10$.

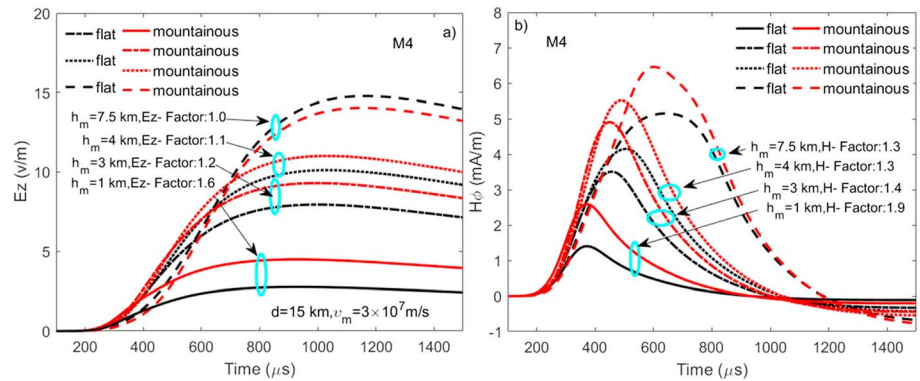


Figure 9. Vertical electric field (a) and azimuthal magnetic field (b) at 15 km associated with the M-component-type pulse M4 (shown in Figure 7), calculated for different junction point heights (1, 3, 4, and 7.5 km). Black curves: simulated fields along an assumed flat lossy ground. Red curves: simulated fields considering the mountainous topography between the Säntis Tower and the field measurement sensor in Herisau. Current wave velocity 3×10^7 m/s. Ground reflection coefficient $\rho_g = 0.8$. Ground electrical parameters: $\sigma = 1$ mS/m, $\epsilon_r = 10$.

differ from those for return strokes, because of a different current distribution and different current waveform characteristics.

For the analysis, we will define the propagation factor as the ratio of the field peak evaluated along the mountainous terrain to the field peak evaluated for a flat terrain. These factors for the vertical electric field and the azimuthal magnetic field are

$$\begin{aligned} \text{Ez-Factor} &= \text{Ez}_{\text{peak}}(\text{mountainous}) / \text{Ez}_{\text{peak}}(\text{flat}) \\ \text{H-Factor} &= \text{H}_{\text{peak}}(\text{mountainous}) / \text{H}_{\text{peak}}(\text{flat}) \end{aligned} \quad (4)$$

We have selected for the analysis four typical current waveforms with different risetimes, based on the study of He, Azadifar, Rachidi, et al. (2018). The current waveforms are shown in Figure 7.

Figure 8 illustrates the effect of the M-component-type current wave velocity on the electric and magnetic fields at 15 km, considering the channel base current pulse M1 (shown in Figure 7). The calculations were performed (i) considering a flat, finite-conductivity ground and (ii) taking into account mountainous topography, as described in section 3.3. The considered velocities for the M-component wave are 1×10^7 , 2×10^7 , 3×10^7 , and 1×10^8 m/s (Jordan et al., 1995; Rakov et al., 1995). The height of the junction point was assumed to be $h_m = 5$ km, the ground reflection coefficient for current was assumed to be $\rho_g = 0.8$, and the ground electrical parameters were set to $\sigma = 1$ mS/m, $\epsilon_r = 10$. Considering the rocky terrain at the summit of the Säntis Tower (Romero et al., 2013), a ground reflection coefficient of 0.8 (rather than 1 used previously) was used here.

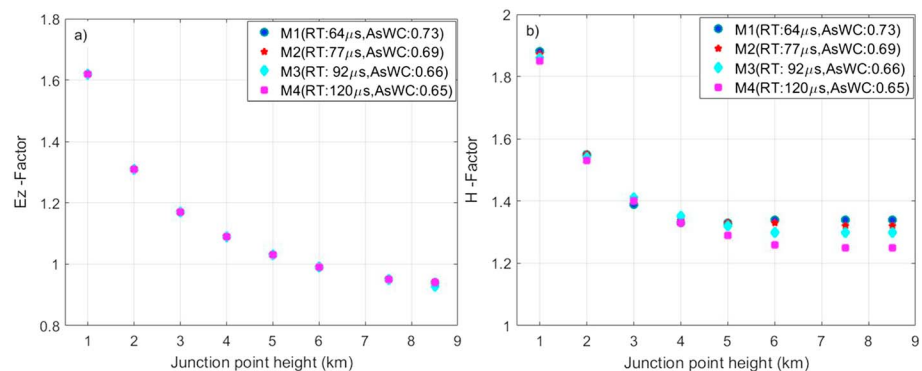


Figure 10. Propagation factors for the vertical electric field (a) and magnetic field (b) at 15 km associated with the considered component waveforms M1, M2, M3, and M4 shown in Figure 7. The results are presented as a function of the junction point height.

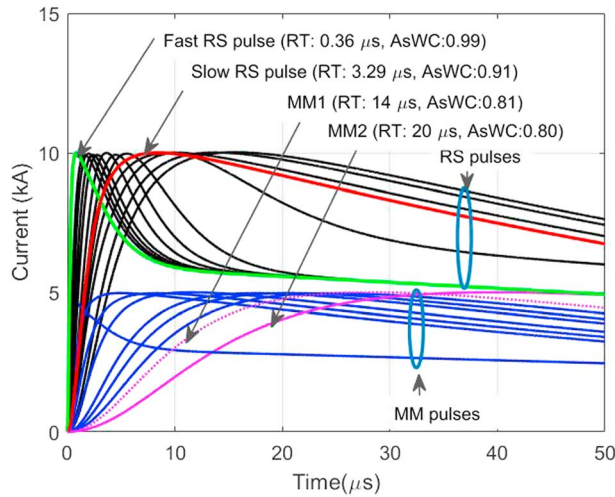


Figure 11. Typical current waveforms associated with return stroke pulses and mixed-mode pulses. Two return stroke pulses (*fast RS pulse* shown in green and *slow RS pulse* shown in red) and two mixed-mode pulses (MM1 and MM2 shown in solid and dashed pink) are used to compute the electric and magnetic fields shown in Figures 12 and 13. The parameters of the waveforms (risetime and AsWC) are given in the figure.

The following conclusions can be drawn from the presented simulation results:

1. As can be seen in Figure 8, the velocity of the M-component pulse has a significant effect on the risetime of the electromagnetic fields. A higher traveling wave speed results in larger magnetic field peaks. However, the peak of the electric field at 15 km seems to be insensitive to the M-component wave speed, which is different from the trend seen for magnetic field. This can be explained by the fact that at this distance, the electric field is dominated by the static component (see Figure 5a), which appears to mainly depend on the overall transferred charge. Note that this is in contrast with the static component of return stroke field, which is inversely proportional to the velocity (see Table 5.2 of Rakov, 2016a). The enhancement factors for H-field in the range from 1.3 to 1.6 are reported in panel b for each case.
2. Effect of the mountainous terrain on the electric field enhancement for the considered junction point height is negligible. It has also an insignificant impact on the early time response of the magnetic field, which is dominated by the downward incident wave. The effect of the mountainous terrain becomes significant after the downward wave has reached the ground and when the ground-reflected wave is launched. This can be clearly seen in

Figure 8b. For example, when the velocity is 1×10^7 m/s, the wave reaches the ground at $500 \mu\text{s}$, which is the time when the effect of the mountainous terrain becomes important.

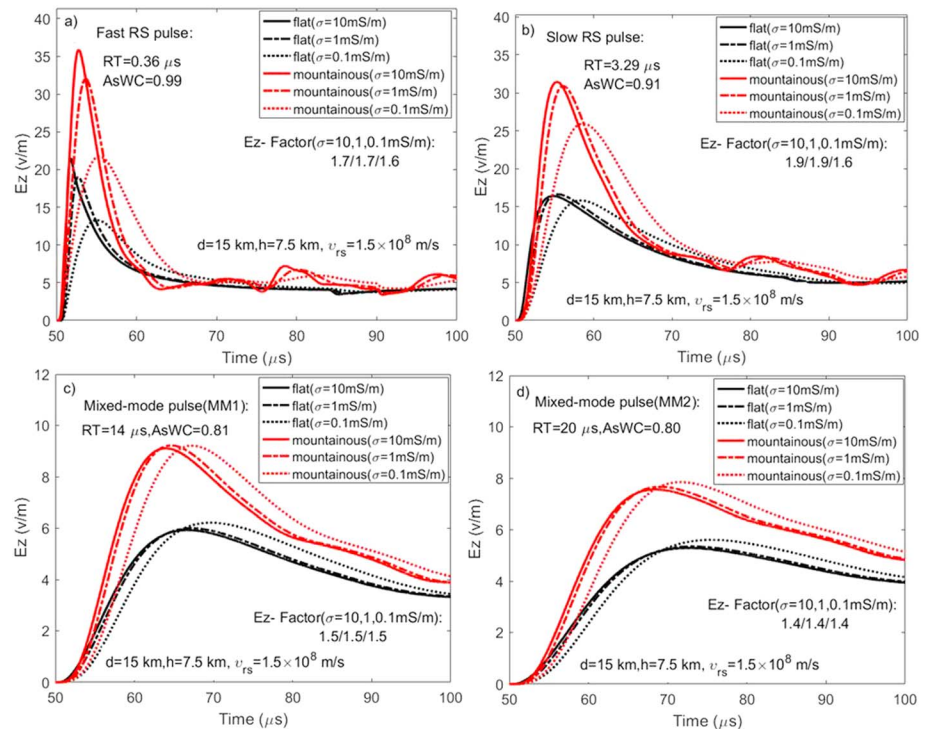


Figure 12. Vertical electric fields at 15 km associated with the return-stroke pulses and mixed-mode pulses shown in Figure 11. (a) Fast return stroke, (b) slow return stroke, (c) mixed-mode pulse (MM1), and (d) mixed-mode pulse (MM2). Solid curves: $\sigma = 10$ mS/m; dashed curves: $\sigma = 1$ mS/m; dotted curves: $\sigma = 0.1$ mS/m. Black curves: simulated fields along a flat lossy ground. Red curves: simulated fields considering the mountainous topography between the Sântis Tower and the field measurement sensor in Herisau. Return stroke and mixed-mode speed $v_{rs} = 1.5 \times 10^8$ m/s. Attenuation height constant $\lambda = 2$ km.

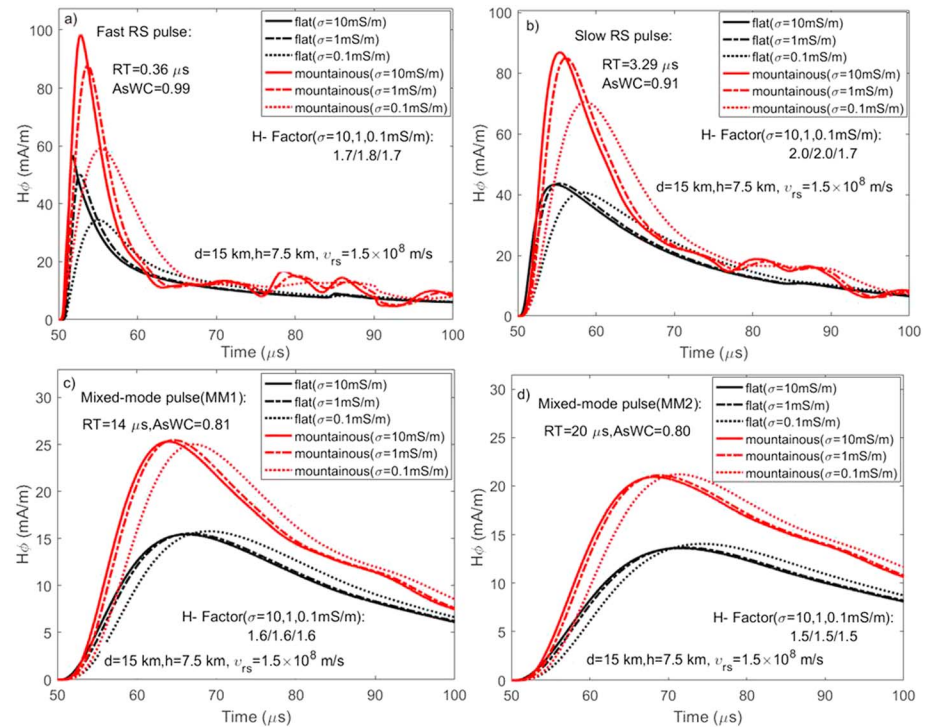


Figure 13. Azimuthal magnetic fields at 15 km associated with the return-stroke pulses and mixed-mode pulses shown in Figure 11. (a) Fast return stroke, (b) slow return stroke, (c) mixed-mode pulse (MM1), and (d) mixed-mode pulse (MM2). Solid curves: $\sigma = 10$ mS/m; dashed curves: $\sigma = 1$ mS/m; dotted curves: $\sigma = 0.1$ mS/m. Black curves: simulated fields along a flat lossy ground. Red curves: simulated fields considering the mountainous topography between the S antis Tower and the field measurement sensor in Herisau. The return stroke and mixed-mode speed is $v_{rs} = 1.5 \times 10^8$ m/s. The attenuation height constant is $\lambda = 2$ km.

As mentioned in section 1, an M-component-type pulse is believed to be associated with the reactivation of a decayed branch or the connection of a newly created channel to the ICC/CC-carrying channel to ground at high junction points (>1 km; Zhou et al., 2015). In Figure 9, we examine the effect of the height of the junction points on the electric and magnetic fields at 15 km, this time using the channel base current waveform M4, in order to examine the impact of different current waveform parameters on the propagation factors (see Figure 7). The calculations were again performed considering either a flat ground or taking into account the mountainous terrain. The considered values for height of the junction point were 1, 3, 4, and 7.5 km. The M-component wave speed was assumed to be 3×10^7 m/s, and the ground electrical parameters were as follows: $\sigma = 1$ mS/m, $\epsilon_r = 10$.

The results show that the propagation factors (defined by equations (4)) decrease as the junction point height increases. When the junction point height is as high as 7.5 km, the Ez-Factor becomes 0.95, which means that the mountainous terrain results in a slight attenuation of the electric field peak. For a junction height of 1 km, the propagation factor for the electric field becomes 1.62, approaching the value of 1.8 inferred by Li, Azadifar, Rachidi, Rubinstein, Paolone, et al. (2016) for return strokes and mixed-mode pulses. It is worth noting that according to Zhou et al. (2015), junction points lower than 1 km or so would result in a mixed-mode transfer of charge in which a downward leader/return stroke-like process is believed to take place.

Figure 10 shows the propagation factors for the electric and magnetic fields as defined in equations (4) as a function of the junction point height and for the considered four M-component pulses, which are characterized by different risetimes (and slightly different AsWC). It can be seen from the figures that both electric and magnetic field propagation factors are not very sensitive to the risetimes and AsWC of the current pulses. However, the results confirm the high variability of the propagation factors as a function of the junction point height. For junction point heights of about 1 km, the propagation factors reach a value of about 1.6

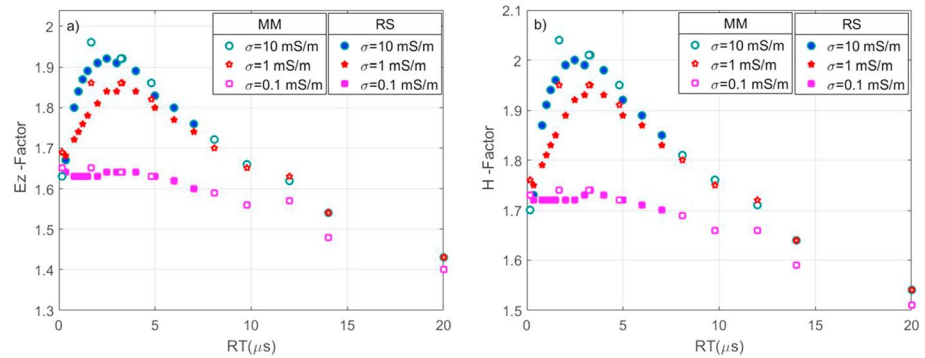


Figure 14. Propagation factors for the vertical electric field (a) and for the magnetic field (b) at 15 km associated with 13 return-stroke pulses and 9 mixed-mode pulses as a function of the current risetime. Three different ground conductivities are considered: (i) $\sigma = 10$ mS/m (blue filled circles), (ii) $\sigma = 1$ mS/m (red filled pentagram), and $\sigma = 0.1$ mS/m (pink filled rectangles).

(for the E-field) and 1.9 (for the H-field). For a junction height higher than 6 km, the E-field propagation factor becomes slightly lower than 1.

4.4. Comparison With Return-Stroke Pulses and Mixed-Mode Pulses

As mentioned in section 4.3, the effect of the mountainous terrain on the propagation of electromagnetic fields from lightning return strokes to the Säntis Tower was analyzed by Li, Azadifar, Rachidi, Rubinstein, Paolone, et al. (2016), where it was shown that the propagation of the field along the mountainous terrain between the Säntis Tower and the field observation point results in a significant enhancement of the vertical electric field associated with return-stroke-type pulses, compared to the case of the propagation along a flat ground. The aim of this section is to present a more extensive analysis of the mountainous terrain on return stroke (RS) and mixed-mode (MM) pulses, as a function of the current risetime and AsWC. To do this, we have considered 13 RS pulses with risetimes ranging from 0.36 to 7.0 μ s (AsWC from 0.87 to 0.99) and 9 MM pulses with risetimes ranging from 0.15 to 20 μ s (AsWC from 0.80 to 0.99). The range of variation of the risetimes is based on the experimental analysis of He, Azadifar, Rachidi, et al. (2018). The peak value of all the RS pulses was considered to be 10 kA, while that of MM pulses were assumed to be 5 kA. These values correspond to the arithmetic mean values derived in He, Azadifar, Rachidi, et al. (2018). The considered RS and MM pulses are shown in Figure 11

Four pulses including two typical return-stroke pulses (labeled as *fast risetime RS pulse* and *slow risetime RS pulse*) and two mixed-mode pulses (labeled as MM1 and MM2) are highlighted in Figure 11. Figures 12 and 13 present the computed electric and magnetic field waveforms at 15 km for the same four pulses,

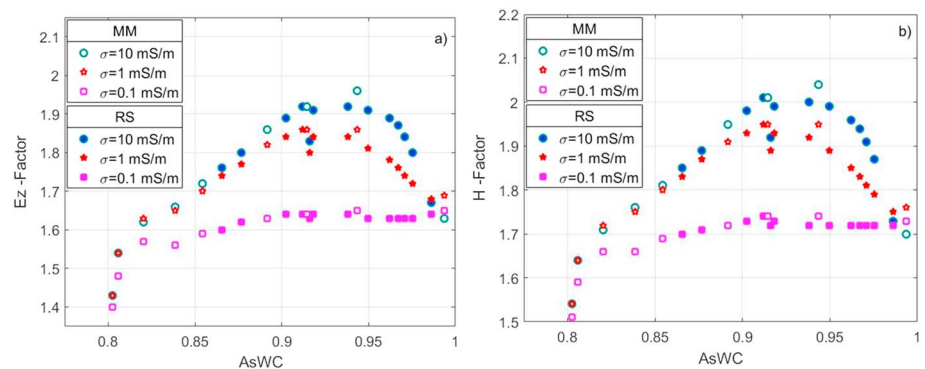


Figure 15. Propagation factors for the vertical electric field (a) and for the magnetic field (b) at 15 km associated with 13 return-stroke pulses and 9 mixed-mode pulses as a function of the asymmetrical waveform coefficients (AsWCs). Three different ground conductivities are considered: (i) $\sigma = 10$ mS/m (blue filled circles), (ii) $\sigma = 1$ mS/m (red filled pentagram), and $\sigma = 0.1$ mS/m (pink filled rectangles).

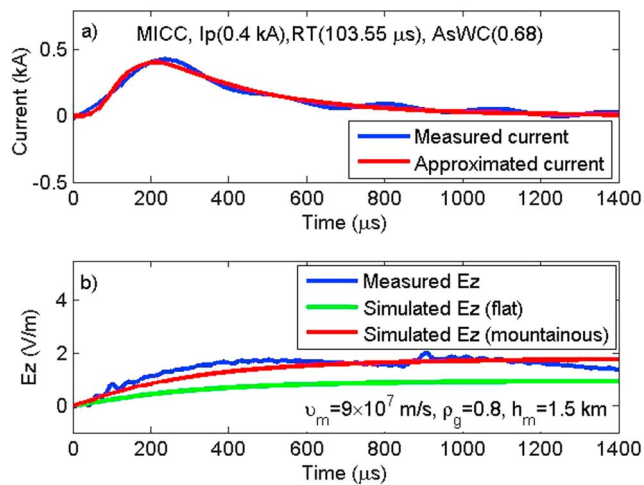


Figure 16. Measured and computed vertical electric fields at 15 km produced by an M-component-type ICC pulse belonging to an upward negative lightning that occurred on 18 August 2016 at 18:49:29. (a) Measured current waveform (after applying a low-pass filter with a cutoff frequency of 10 kHz) and analytical approximation. (b) Measured E-field waveform (after applying a low-pass filter with a cutoff frequency of 400 kHz) and simulated results obtained assuming a flat ground (green) and taking into account the mountainous terrain (red). Ground parameters: $\sigma = 10$ mS/m, relative permittivity $\epsilon_r = 10$.

Figure 14 presents the propagation factors for the electric and magnetic fields for 13 return-stroke pulses and 9 mixed-mode pulses as a function of the current risetime, and for three different ground conductivities. It can be seen that the field enhancement (propagation factor) is higher for larger ground conductivities. It can also be seen that the enhancement effect tends to decrease with increasing current risetime, except for very short risetimes (less than 2.5 μ s or so) where the tendency reverses. We believe

that this reversal of the trend for fast risetimes is essentially due to the irregular propagation path. Indeed, by considering a perfectly smooth propagation path between the Sântis Tower and the observation point, represented by a conical shape, the resulting propagation factors would be in the range of 1 to 1.2 and remain quasi-constant as a function of the risetime.

considering either a flat conducting ground or taking into account the mountainous propagation path, as described in section 3.3. The return stroke and mixed-mode speeds are assumed to be 1.5×10^8 m/s and the current attenuation constant $\lambda = 2$ km. Three different values for the ground conductivity have been considered, namely, 10, 1, and 0.1 mS/m.

From Figure 12 one can see that, as expected, the finite ground conductivity has a significant effect on the peak value and risetime of the vertical electric field for the fast pulse. The effect of the finite ground conductivity on the slow RS and mixed-mode pulses is much less significant, because of the less significant higher-frequency content of their spectrum. Furthermore, the mountainous terrain between the Sântis Tower and the field observation point in Herisau results in an enhancement of the field for all the considered pulses, consistent with the findings of Li, Azadifar, Rachidi, Rubinstein, Paolone, et al. (2016). However, the amount of enhancement depends on the current waveform and on the ground electric conductivity. Specifically, the propagation factor decreases with decreasing conductivity.

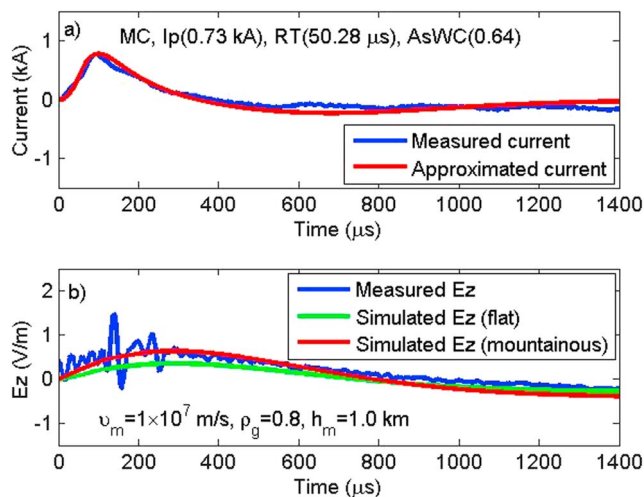


Figure 17. Measured and computed vertical electric fields at 15 km produced by a classical M component belonging to an upward negative lightning that occurred on 18 August 2016 at 15:38:58. The same filters were employed as in Figure 16. (a) Measured current waveform and analytical approximation. (b) Measured E-field waveform (blue) and simulated results obtained assuming a flat ground (green) and taking into account the mountainous terrain (red). Ground parameters: $\sigma = 10$ mS/m, relative permittivity $\epsilon_r = 10$.

The results for the magnetic fields presented in Figure 13 are very similar to those obtained for the electric field. The values for the H-field propagation factors are slightly higher than for the E-field, presumably because the static component of the electric field still contributes to the electric field peak at that distance.

Figure 15 presents similar results but as a function of the AsWC. It can be seen that the enhancement factors for both electric field and magnetic field tend to increase with increasing values of AsWC, except for values higher than about 0.95 where an opposite effect is observed. Values of AsWC of 0.95 or higher correspond to steep fronts (short risetimes).

5. Comparison Between Model-Predicted Fields and Observations

In this section, we present a comparison between the model-predicted fields and experimental observations at the Sântis Tower. We have selected four pulses belonging to two upward flashes that occurred on 18 August 2016 at 15:38:58 and 18:49:29 (local time). Each pulse is associated with a different charge transfer mode, namely, return stroke, mixed mode, classical M component, and M-component-type ICC. The measured current waveforms at the channel base were represented analytically using exponential functions with parameters determined by a genetic algorithm approach (Bermudez et al., 2002). The results are presented in Figures 16–19, in which the blue curves show the measured

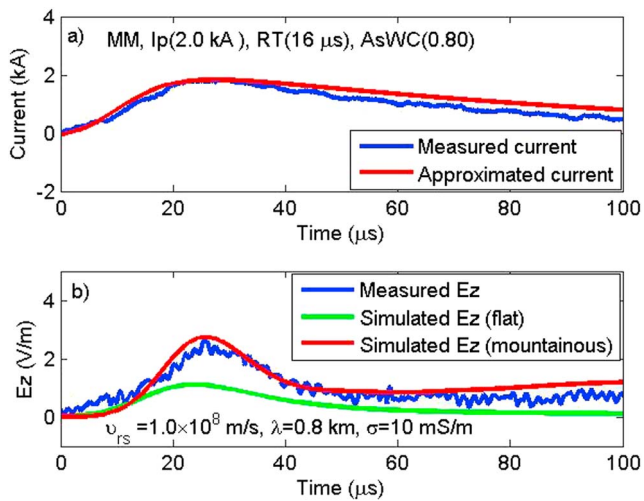


Figure 18. Measured and computed vertical electric fields at 15 km produced by a mixed-mode pulse belonging to an upward negative lightning that occurred on 18 August 2016 at 18:49:29. (a) Measured current waveform and analytical approximation. (b) Measured E-field waveform (blue) and simulated results obtained assuming a flat ground (green) and taking into account the mountainous terrain (red). Ground parameters: $\sigma = 10$ mS/m, relative permittivity $\epsilon_r = 10$.

risetime is 50.3 μ s, and its asymmetrical waveform coefficient (AsWC) is 0.64. It can be seen in Figure 17 b that the vertical electric field waveform simulated considering the mountainous terrain matches very well the measured data. The adopted parameters of the model are given in Figure 17b. In this case, the mountainous terrain effect enhances the vertical electric field by a factor of about 1.65. This is consistent with the discussion presented in section 4.3, in which it was shown that the electric field propagation factor is around 1.7 for a junction point height of about $h_m = 1$ km.

Figure 18 presents the comparison of the approximated current waveform and the simulated vertical electric field at 15 km with the experimental observation of a mixed-mode pulse associated with an upward

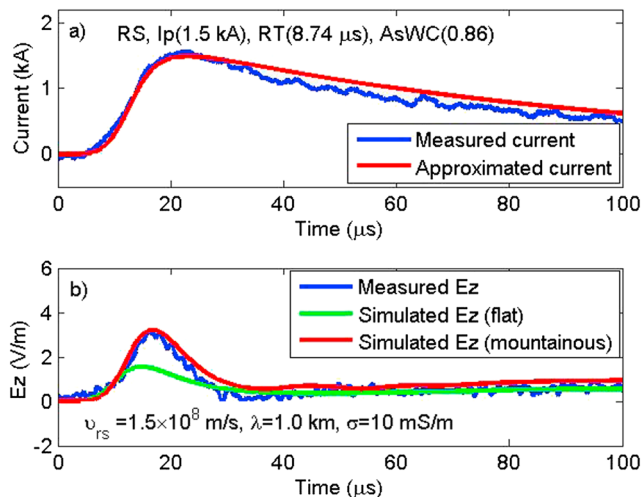


Figure 19. Measured and computed vertical electric fields at 15 km produced by a return-stroke pulse belonging to an upward negative lightning that occurred on 18 August 2016 at 15:38:58. (a) Measured current waveform and analytical approximation. (b) Measured E-field waveform (blue) and simulated results obtained assuming a flat ground (green) and taking into account the mountainous terrain (red). Ground parameters: $\sigma = 10$ mS/m, relative permittivity $\epsilon_r = 10$.

negative lightning that occurred on 18 August 2016 at 18:49:29. The peak of the measured current pulse is 0.4 kA, its 10–90% risetime is 103.5 μ s, and its AsWC is 0.68. The parameters of the model (shown in the figure) were adjusted in order to provide the best match with the measured field waveform. One can see from Figure 16b that the electric field waveform simulated considering the mountainous terrain matches quite well the observed data. It can also be seen that considering a flat lossy ground results in an underestimation of the field peak by 30%, consistent with the vertical E-field propagation factors inferred in section 4.3 for the considered junction point height.

Figure 17 presents the comparison of the approximated current waveform and the simulated vertical electric field at 15 km with the experimental observation of a classical M-component pulse associated with an upward negative lightning that occurred on 18 August 2016 at 15:38:58. The peak of the measured current pulse is 0.73 kA, its 10–90%

risetime is 50.3 μ s, and its asymmetrical waveform coefficient (AsWC) is 0.64. It can be seen in Figure 17 b that the vertical electric field waveform simulated considering the mountainous terrain matches very well the measured data. The adopted parameters of the model are given in Figure 17b. In this case, the mountainous terrain effect enhances the vertical electric field by a factor of about 1.65. This is consistent with the discussion presented in section 4.3, in which it was shown that the electric field propagation factor is around 1.7 for a junction point height of about $h_m = 1$ km.

Figure 18 presents the comparison of the approximated current waveform and the simulated vertical electric field at 15 km with the experimental observation of a mixed-mode pulse associated with an upward negative lightning that occurred on 18 August 2016 at 18:49:29. The peak of the measured current is 2 kA, its 10–90% risetime is 16 μ s, and its AsWC is 0.8. From Figure 18b one can see that the vertical electric field waveform simulated considering the mountainous terrain is in very good agreement with the observed data. The adopted parameters of the model are given in Figure 18b. Considering a flat lossy ground results in an underestimation of the peak field by about 40% or so, which is consistent with the analysis presented in section 4.4 and the findings of Li, Azadifar, Rachidi, Rubinstein, Paolone, et al. (2016).

Figure 19 presents the comparison of the approximated current waveform and the simulated vertical electric field at 15 km with the experimental observation of a return stroke pulse associated with an upward negative lightning that occurred on 18 August 2016 at 15:38:58. The peak of the measured current is 1.5 kA, its 10–90% risetime is 8.7 μ s, and its AsWC is 0.86. Figure 19b shows that the electric field waveform simulated considering the mountainous terrain is in excellent agreement with the observed data. The adopted parameters of the model are given in Figure 19b. The assumption of a flat ground results in an underestimation of the peak value by 35% or so, which is consistent with the analysis presented in section 4.4.

Table 1 summarizes the parameters of the models, namely, v_{rs} and λ for return-stroke and mixed-mode pulses, and v_m , h_m , and ρ_g for M

Table 1
Summary of Parameters Derived From Matching Simulated and Measured Field

Parameters of M component	Pulse type		Comparison with previous studies	
	MICC	MC	References	Comparison results
Charge transfer mode				
$v_m/(\times 10^7 \text{ m/s})$	9.0	1.0	Rakov et al. (1995) and Jordan et al. (1995)	In its inferred range
h_m/km	1.5	1.0	Zhou et al. (2015)	Agree with the observation
ρ_g	0.8	0.8	Romero et al. (2013)	Agree with the observation
Parameters of return stroke	Pulse type		Comparison with previous studies	
Charge transfer mode	RS	MM	References	Comparison results
$v_{rs}/(\times 10^8 \text{ m/s})$	1.5	1.0	Idone and Orville (1982) and Rakov (2007)	In its inferred range
λ/km	1.0	0.8	Nucci et al. (1988) and Nucci and Rachidi (1989)	Lower than the proposed

components and M-component-type ICC pulses, which were adjusted to match the simulation results with the experimental data.

The junction point heights for the M-component pulse and M-component ICC pulse adopted in the model were 1.0 and 1.5 km, respectively. These values are in agreement with the studies of Zhou et al. (2015) according to which the height of the junction point should be higher than 1 km for the M-component charge transfer to ground. The adopted value for the ground reflection coefficient is 0.8. Assuming a channel impedance of about 0.5 to 2.5 k Ω (Rakov, 1998), this would correspond to a grounding impedance of about 50 to 300 Ω , which is reasonable considering the rocky terrain at the summit of the Sântis mountain (with a resistivity as high as 10 k Ω .m (Romero et al., 2013)). The velocities for the M-component pulse and M-component-type ICC pulse are in the range of typical speeds for M components (Jordan et al., 1995; Rakov et al., 1995). The adopted propagation speeds for the return-stroke and mixed-mode pulses are in the range of the experimentally observed return stroke speeds (e.g., Idone & Orville, 1982; Rakov, 2007). However, the values for the current decay height constant adopted in the model (1.0 km for the return stroke and 0.8 km for the mixed-mode pulse) are lower than the typical value of 2.0 km suggested in Nucci et al. (1988) and Nucci and Rachidi (1989). This lower attenuation height constant may indicate a more severe attenuation of the lightning current propagating along the channel in an upward flash compared to a downward flash. The value for the ground conductivity considered in all the four cases is 10 mS/m, in agreement with Li, Azadifar, Rachidi, Rubinstein, Paolone, et al. (2016).

6. Summary and Conclusions

We analyzed the propagation effect of mountainous terrain on the electromagnetic field associated with the M-component charge transfer mode and compared the results with the propagation effect on the fields associated with the leader/return stroke and mixed charge transfer modes. For the analysis, we used a 2-D FDTD method, in which the M component is modeled by the sequence/superposition of a downward current wave and an upward current wave resulting from the reflection at the bottom of the lightning channel (Rakov et al., 1995 model), and the return-stroke and mixed-mode pulses are modeled adopting the MTLE model. The finite ground conductivity and the mountainous terrain between the Sântis Tower and the field sensor located 15 km away at Herisau were taken into account. The effects of the mountainous propagation path on the electromagnetic fields were examined for classical M-component and M-component-ICC pulses. Use was made of the propagation factors defined as the ratio of the electric or magnetic field peak evaluated for the mountainous terrain to the field peak evaluated for a flat terrain.

The velocity of the M-component pulse was found to have a significant effect on the risetime of the electromagnetic fields. A faster-traveling wave speed results in larger peaks for the magnetic field. However, the peak of the electric field at 15 km appears to be insensitive to the M-component wave speed. This can be explained by the fact that at 15 km, the electric field is still dominated by the static component, which mainly depends on the overall transferred charge. The contribution of the radiation component to the fields at 100 km accounts for about 77% of the peak electric field and 81% of the peak magnetic field, significantly lower compared to the contribution of the radiation component to the return stroke fields at the same distance.

The simulation results showed that neither the electric nor the magnetic field propagation factor is very sensitive to the risetime and AsWC of the current pulse. However, the results indicate a high variability of the propagation factors as a function of the junction point height. For junction point heights of about 1 km, the propagation factors reach a value of about 1.6 (for the E-field) and 1.9 (for the H-field). For a junction height higher than 6 km, the E-field factor becomes slightly lower than 1. The obtained results are consistent with the findings of Li, Azadifar, Rachidi, Rubinstein, Paolone, et al. (2016), in which an electric field propagation factor of 1.8 was inferred for return-stroke and mixed-mode pulses, considering that junction points lower than 1 km or so would result in a mixed-mode transfer of charge, in which a leader/return-stroke-like process is believed to take place.

It was also found that the field enhancement (propagation factor) is higher for larger ground conductivities. Furthermore, the enhancement effect tends to decrease with increasing current risetime, except for very short risetimes (less than 2.5 μ s or so) where the tendency reverses.

Model-predicted fields associated with different charge transfer modes, namely, return stroke, mixed, classical M component, and M-component-type ICC pulse, were compared with experimental observations at the Säntis Tower and at the field measuring station, 15 km away. It was found that the vertical electric field waveforms simulated considering the mountainous terrain are in very good agreement with the observed data. The adopted parameters of the models that provide the best match with the measured field waveforms were consistent with experimental observations. The values for the current decay height constant adopted in the return stroke and mixed-mode models (1.0 km for the return stroke and 0.8 km for the mixed-mode pulse) were lower than the typical value of 2.0 km used in the literature.

Acknowledgments

The lightning current and electric field data measured from Säntis Tower can be obtained from the Electromagnetic Compatibility Laboratory at the Swiss Federal Institute of Technology (EPFL) in Lausanne (<https://emc.epfl.ch/>), Switzerland.

References

- Azadifar, M., Paolone, M., Pavanello, D., Rachidi, F., Rakov, V. A., Romero, C., & Rubinstein, M. (2014). An update on the characteristics of positive flashes recorded on the Säntis Tower, paper presented at 2014 International Conference on Lightning Protection (ICLP), IEEE.
- Azadifar, M., Rachidi, F., Rubinstein, M., Rakov, V. A., Paolone, M., Pavanello, D., & Metz, S. (2016). Fast initial continuous current pulses versus return stroke pulses in tower-initiated lightning. *Journal of Geophysical Research: Atmospheres*, *121*, 6425–6434. <https://doi.org/10.1002/2016jd024900>
- Baba, Y., & Rakov, V. A. (2003). On the transmission line model for lightning return stroke representation. *Geophysical Research Letters*, *30*(24), 2294. <https://doi.org/10.1029/2003GL018407>
- Baba, Y., & Rakov, V. A. (2005). On the use of lumped sources in lightning return stroke models. *Journal of Geophysical Research – Atmospheres*, *110*(D3). <https://doi.org/10.1029/2004JD005202>
- Baba, Y., & Rakov, V. A. (2007a). Electromagnetic models of the lightning return stroke. *Journal of Geophysical Research – Atmospheres*, *112*(D4). <https://doi.org/10.1029/2006JD007222>
- Baba, Y., & Rakov, V. A. (2007b). Electromagnetic fields at the top of a tall building associated with nearby lightning return strokes. *IEEE Transactions on Electromagnetic Compatibility*, *49*(3), 632–643. <https://doi.org/10.1109/TEMC.2007.902402>
- Baba, Y., & Rakov, V. A. (2008). Influence of strike object grounding on close lightning electric fields. *Journal of Geophysical Research*, *113*, D12109. <https://doi.org/10.1029/2008JD009811>
- Berenger, J.-P. (2005). Long range propagation of lightning pulses using the FDTD method. *IEEE Transactions on Electromagnetic Compatibility*, *47*(4), 1008–1012. <https://doi.org/10.1109/TEMC.2005.858747>
- Berger, K. (1975). Parameters of lightning flashes. *Electra*, *41*, 23–37.
- Bermudez, J.L., Pena-Reyes, C.A., Rachidi, F., and Heidler, F. (2002). Use of genetic algorithms to extract primary lightning current parameters, paper presented at Proceedings of EMC Europe 2002. International Symposium on Electromagnetic Compatibility. Cooray, V., Engineering, and Technology (2012), Lightning electromagnetics, Institution of Engineering and Technology.
- Diendorfer, D., Pichler, H., & Mair, M. (2009). Some parameters of negative upward-initiated lightning to the Gaisberg Tower (2000–2007). *IEEE Transactions on Electromagnetic Compatibility*, *51*(3), 443–452. <https://doi.org/10.1109/TEMC.2009.2021616>
- Flache, D., Rakov, V., Heidler, F., Zischank, W., & Thottappillil, R. (2009). Leader/return stroke versus M-component mode of charge transfer to ground in initial-stage pulses of upward lightning, paper presented at European COST Action P18, 4th International Symposium on Lightning Physics and Effects. Vienna, Austria. May 25–27 2009.
- He, L., Azadifar, M., Li, Q., Rubinstein, M., Rakov, V. A., Mediano, A., et al. (2018). Modeling of different charge transfer modes in upward flashes constrained by simultaneously measured currents and fields, paper presented at 2018 Joint IEEE EMC and Asia Pacific EMC Symposium.
- He, L., Azadifar, M., Rachidi, F., Rubinstein, M., Rakov, V. A., Cooray, V., et al. (2018). An analysis of current and electric field pulses associated with upward negative lightning flashes initiated from the Säntis Tower. *Journal of Geophysical Research: Atmospheres*, *123*(8), 4045–4059. <https://doi.org/10.1029/2018JD028295>
- He L., Zhang, Q., Xing, H., and Hou, W. (2014). On validation of FCCFs for lightning striking tall objects considering propagation effect of finitely conducting earth, paper presented at 2014 International Conference on Lightning Protection (ICLP), 11–18 Oct. 2014, doi: <https://doi.org/10.1109/iclp.2014.6973391>
- Heidler, F. H., Manhardt, M., & Stimper, K. (2015). Transient response of the top structure of the Peissenberg Tower to lightning. *IEEE Transactions on Electromagnetic Compatibility*, *57*(6), 1547–1555. <https://doi.org/10.1109/TEMC.2015.2481088>
- Idone, V. P., & Orville, R. E. (1982). Lightning return stroke velocities in the Thunderstorm Research International Program (TRIP). *Journal of Geophysical Research*, *87*(C7), 4903–4916. <https://doi.org/10.1029/JC087iC07p04903>
- Jordan, D. M., Idone, V. P., Orville, R. E., Rakov, V. A., & Uman, M. A. (1995). Luminosity characteristics of lightning M components. *Journal of Geophysical Research*, *100*(D12), 25,695–25,700. <https://doi.org/10.1029/95JD01362>

- Khosravi-Farsani, M., Moini, R., Sadeghi, S. H., & Rachidi, F. (2013). On the validity of approximate formulas for the evaluation of the lightning electromagnetic fields in the presence of a lossy ground. *IEEE Transactions on Electromagnetic Compatibility*, *55*(2), 362–370. <https://doi.org/10.1109/TEMC.2012.2211364>
- Kobayashi, S., Suzuki, Y., & Baba, Y. (2016). Lightning electromagnetic field calculation using the constrained interpolation profile method with a subgridding technique. *IEEE Transactions on Electromagnetic Compatibility*, *58*(5), 1682–1685. <https://doi.org/10.1109/TEMC.2016.2575079>
- Li, D., Azadifar, M., Rachidi, F., Rubinstein, M., Diendorfer, G., Sheshyekani, K., et al. (2016). Analysis of lightning electromagnetic field propagation in mountainous terrain and its effects on ToA-based lightning location systems. *Journal of Geophysical Research: Atmospheres*, *121*, 895–911. <https://doi.org/10.1002/2015JD024234>
- Li, D., Azadifar, M., Rachidi, F., Rubinstein, M., Paolone, M., Pavanello, D., et al. (2016). On lightning electromagnetic field propagation along an irregular terrain. *IEEE Transactions on Electromagnetic Compatibility*, *58*(1), 161–171. <https://doi.org/10.1109/TEMC.2015.2483018>
- Li, D., Rubinstein, M., Rachidi, F., Diendorfer, G., Schulz, W., & Lu, G. (2017). Location accuracy evaluation of ToA-based lightning location systems over mountainous terrain. *Journal of Geophysical Research: Atmospheres*, *122*, 11,760–11,775. <https://doi.org/10.1002/2017JD027520>
- Li, D., Zhang, Q., Wang, Z., & Liu, T. (2014). Computation of lightning horizontal field over the two-dimensional rough ground by using the three-dimensional FDTD. *IEEE Transactions on Electromagnetic Compatibility*, *56*(1), 143–148. <https://doi.org/10.1109/temc.2013.2266479>
- Li, Q., Wang, J., Rachidi, F., Rubinstein, M., Šunjerga, A., Cai, L., & Zhou, M. (2019). Importance of taking into account the soil stratification in reproducing the late-time features of distant fields radiated by lightning. *IEEE Transactions on Electromagnetic Compatibility* (Vol. 61, pp. 935–944). <https://doi.org/10.1109/TEMC.2018.2840702>
- Malan, D., & Collens, H. (1937). Progressive lightning III—The fine structure of return lightning strokes. *Proceedings of the Royal Society of London A*, *162*(909), 175–203. <https://doi.org/10.1098/rspa.1937.0175>
- Meyer, D. (2011). In T. Tachikawa, M. Kaku, A. Iwasaki, D. B. Gesch, M. J. Oimoen, Z. Zhang, J. J. Danielson, T. Krieger, B. Curtis, J. Haase, M. Abrams, & C. Carabajal (Eds.), *ASTER Global Digital Elevation Model Version 2—Summary of validation results* (p. 27). Washington, DC: NASA.
- Mimouni, A., Rachidi, F., & Azzouz, Z.-E. (2008). A finite-difference time-domain approach for the evaluation of electromagnetic fields radiated by lightning strikes to tall structures. *Journal of Electrostatics*, *66*(9–10), 504–513. <https://doi.org/10.1016/j.elstat.2008.05.002>
- Mosaddeghi, A., Pavanello, D., Rachidi, F., Rubinstein, M., & Zweigacker, P. (2009). Effect of nearby buildings on electromagnetic fields from lightning. *Journal of Lightning Research*, *1*(1), 52–60. <https://doi.org/10.2174/1652803400901010052>
- Mur, A. (1981). Absorbing boundary conditions for the finite-difference approximation of the time-domain electromagnetic-field equations. *IEEE Transactions on Electromagnetic Compatibility*, *EMC-23*(4), 377–382. <https://doi.org/10.1109/TEMC.1981.303970>
- Nucci, C. A., Mazzetti, C., Rachidi, F., & Ianoz, M. (1988). On lightning return stroke models for LEMP calculations, paper presented at 19th International Conference on lightning protection.
- Nucci, C. A., and Rachidi, F. (1989). Experimental validation of a modification to the Transmission Line model for LEMP calculation, paper presented at 8th Symposium and Technical Exhibition on Electromagnetic Compatibility.
- Oikawa, T., Sonoda, J., Sato, M., Honma, N., & Ikegawa, Y. (2013). Analysis of lightning electromagnetic field on large-scale terrain model using three-dimensional MW-FDTD parallel computation. *Electrical Engineering in Japan*, *184*(2), 20–27. <https://doi.org/10.1002/ej.22368>
- Pichler, H., Diendorfer, G., & Mair, M. (2010). Some parameters of correlated current and radiated field pulses from lightning to the Gaisberg Tower. *IEEJ Transactions on Electrical and Electronic Engineering*, *5*(1), 8–13. <https://doi.org/10.1002/tee.20486>
- Qie, X., Jiang, R., Wang, R., Yang, J., Wang, J., & Liu, D. (2011). Simultaneously measured current, luminosity, and electric field pulses in a rocket-triggered lightning flash. *Journal of Geophysical Research*, *116*, D10102. <https://doi.org/10.1029/2010JD015331>
- Rachidi, F., & Nucci, C. A. (1990). On the Master, Uman, Lin, Standler and the modified transmission line lightning return stroke current models. *Journal of Geophysical Research*, *95*(D12), 20,389–20,393. <https://doi.org/10.1029/JD095iD12p20389>
- Rachidi, F., Rakov, V. A., Nucci, C. A., & Bermudez, J. L. (2002). Effect of vertically extended strike object on the distribution of current along the lightning channel. *Journal of Geophysical Research*, *107*(D23), 4699. <https://doi.org/10.1029/2002JD002119>
- Rachidi, F., & Thottappillil, R. (1993). Determination of lightning currents from far electromagnetic fields. *Journal of Geophysical Research*, *98*(D10), 18,315–18,321. <https://doi.org/10.1029/93JD01616>
- Rakov, V. A. (1998). Some inferences on the propagation mechanisms of dart leaders and return strokes. *Journal of Geophysical Research*, *103*(D2), 1879–1887. <https://doi.org/10.1029/97JD03116>
- Rakov, V. A. (2007). Lightning return stroke speed. *Journal of Lightning Research*, *1*, 80–89.
- Rakov, V. A. (2016a). Calculation of lightning electromagnetic fields. In *Fundamentals of Lightning*, (pp. 115–126). Cambridge: Cambridge University Press. <https://doi.org/10.1017/CBO9781139680370.006>
- Rakov, V. A. (2016b). Glossary. In *Fundamentals of lightning* (pp. 236–237). Cambridge: Cambridge University Press. <https://doi.org/10.1017/CBO9781139680370.020>
- Rakov, V. A. (2016c). Properties of the downward negative lightning discharge to ground. In *Fundamentals of Lightning* (pp. 52–114). Cambridge: Cambridge University Press. <http://doi.org/10.1017/CBO9781139680370.005>
- Rakov, V. A., Crawford, D. E., Rambo, K. J., Schnetzer, G. H., Uman, M. A., & Thottappillil, R. (2001). M-component mode of charge transfer to ground in lightning discharges. *Journal of Geophysical Research*, *106*(D19), 22,817–22,831. <https://doi.org/10.1029/2000JD000243>
- Rakov, V. A., Thottappillil, R., & Uman, M. A. (1992). On the empirical formula of Willett et al. relating lightning return-stroke peak current and peak electric field. *Journal of Geophysical Research*, *97*(D11), 11,527–11,533. <https://doi.org/10.1029/92JD00720>
- Rakov, V. A., Thottappillil, R., Uman, M. A., & Barker, P. P. (1995). Mechanism of the lightning M component. *Journal of Geophysical Research*, *100*(D12), 25,701–25,710. <https://doi.org/10.1029/95JD01924>
- Romero, C., Mediano, A., Rubinstein, A., Rachidi, F., Rubinstein, M., Paolone, M., et al. (2010). Measurement of lightning currents using a combination of Rogowski coils and B-Dot sensors, paper presented at Lightning Protection (ICLP), 2010 30th International Conference on, IEEE.
- Romero, C., Rachidi, F., Paolone, M., & Rubinstein, M. (2013). Statistical distributions of lightning currents associated with upward negative flashes based on the data collected at the Sántis (EMC) Tower in 2010 and 2011. *IEEE Transactions on Power Delivery*, *28*(3), 1804–1812. <https://doi.org/10.1109/TPWRD.2013.2254727>
- Shoory, A., Rachidi, F., & Cooray, V. (2012). Propagation effects on electromagnetic fields generated by lightning return strokes: Review of simplified formulas and their validity assessment, *Rep.*, IET.

- Shoory, A., Rachidi, F., Delfino, F., Procopio, R., & Rossi, M. (2011). Lightning electromagnetic radiation over a stratified conducting ground: 2. Validity of simplified approaches. *Journal of Geophysical Research*, *116*, D11115. <https://doi.org/10.1029/2010JD015078>
- Soto, E., Perez, E., & Herrera, J. (2014). Electromagnetic field due to lightning striking on top of a cone-shaped mountain using the FDTD. *IEEE Transactions on Electromagnetic Compatibility*, *56*(5), 1112–1120. <https://doi.org/10.1109/TEMC.2014.2301138>
- Thottappillil, R., Goldberg, J. D., Rakov, V. A., Uman, M. A., Fisher, R. J., & Schnetzer, G. H. (1995). Properties of M components from currents measured at triggered lightning channel base. *Journal of Geophysical Research*, *100*(D12), 25,711–25,720. <https://doi.org/10.1029/95JD02734>
- Tran, T. H., Baba, Y., Somu, V. B., & Rakov, V. A. (2017). FDTD modeling of LEMP propagation in the Earth-ionosphere waveguide with emphasis on realistic representation of lightning source. *Journal of Geophysical Research: Atmospheres*, *122*, 12,918–12,937. <https://doi.org/10.1002/2017JD027305>
- Uman, M. A., McLain, D. K., & Krider, E. P. (1975). The electromagnetic radiation from a finite antenna. *American Journal of Physics*, *43*(1), 33–38. <https://doi.org/10.1119/1.10027>
- Visacro, S., Soares, A., Schroeder, M. A. O., Cherchiglia, L. C. L., & de Sousa, V. J. (2004). Statistical analysis of lightning current parameters: Measurements at Morro do Cachimbo Station. *Journal of Geophysical Research*, *109*, D01105. <https://doi.org/10.1029/2003JD003662>
- Yee, K. (1966). Numerical solution of initial boundary value problems involving Maxwell's equations in isotropic media. *IEEE Transactions on Antennas and Propagation*, *14*(3), 302–307. <https://doi.org/10.1109/TAP.1966.1138693>
- Zhang, Q., He, L., Ji, T., & Hou, W. (2014). On the field-to-current conversion factors for lightning strike to tall objects considering the finitely conducting ground. *Journal of Geophysical Research: Atmospheres*, *119*, 8189–8200. <https://doi.org/10.1002/2014jd021496>
- Zhang, Q., Jing, X., Yang, J., Li, D., & Tang, X. (2012). Numerical simulation of the lightning electromagnetic fields along a rough and ocean-land mixed propagation path. *Journal of Geophysical Research*, *117*, D20304. <https://doi.org/10.1029/2012JD017851>
- Zhou, H., Diendorfer, D., Thottappillil, R., Pichler, H., and Mair, M. (2011). Mixed mode of charge transfer to ground for initial continuous current pulses in upward lightning, paper presented at Lightning (APL), 2011 7th Asia-Pacific International Conference on, IEEE.
- Zhou, H., Rakov, V. A., Diendorfer, G., Thottappillil, R., Pichler, H., & Mair, M. (2015). A study of different modes of charge transfer to ground in upward lightning. *Journal of Atmospheric and Terrestrial Physics*, *125-126*, 38–49. <https://doi.org/10.1016/j.jastp.2015.02.008>